Toward the final optical design MOONS, the Multi-Object Optical and Near infrared Spectrometer for the VLT

Oliva, E., Delabre, B., Tozzi, A., Ferruzzi, D., Lee, D., et al.

E. Oliva, B. Delabre, A. Tozzi, D. Ferruzzi, D. Lee, I. Parry, P. Rees II, "Toward the final optical design MOONS, the Multi-Object Optical and Near infrared Spectrometer for the VLT," Proc. SPIE 9908, Ground-based and Airborne Instrumentation for Astronomy VI, 99087R (9 August 2016); doi: 10.1117/12.2231388

SPIE.

Event: SPIE Astronomical Telescopes + Instrumentation, 2016, Edinburgh, United Kingdom

Toward the final optical design of MOONS, the Multi-Object Optical and Near-Infrared spectrograph for the VLT

E. Oliva*[a], B. Delabre[b], A. Tozzi[a] , D. Ferruzzi[a], D. Lee[c], I. Parry[d], P. Rees[c]

[a] INAF-Arcetri Observatory, largo E. Fermi 5, I-50125 Firenze, Italy;
[b] ESO, Karl Schwarzschild str. 2, D-85748 Garching bei Muenchen, Germany;
[c] STCF UK-ATC, Royal Observatory, Blackford Hill, Edinburgh, EH9 3HJ, UK;
[d] Institute of Astronomy, University of Cambridge, Madingley Road, Cambridge CB3 0HA, UK;

ABSTRACT

MOONS (Multi-Object Optical and Near-infrared Spectrograph for the VLT) is entering into the final design phase. This paper presents and discusses the latest proposed version of the optical design of the cryogenic spectrograph. The main developments and modifications were aimed at minimizing the overall size and mass of the cryogenic spectrograph. The most remarkable new feature is the design of an extremely fast (F/0.95), light and compact (40 kg in less than 80 dm^3) camera with superb image quality over a very large field of view (9 degrees on a collimated beam of 265 mm). The camera consists of only three optical elements: two lenses and one mirror. All elements are made of fused-silica. The optical performances are independent on the temperature, i.e. the camera can be fully characterized at room temperatures.

Keywords: Ground-based instruments, multi-object infrared spectrographs

1. INTRODUCTION

MOONS is the acronym of Multi-Object Optical and Near-infrared Spectrograph which is currently being developed for the European Southern Observatory (ESO). The instrument was first selected by ESO[1] in 2011. The phase-A and Preliminary Design Review (PDR) were successfully completed in April 2013 and March 2016, respectively.
The main scientific aims of the instrument[2] include galactic archaeology (based on a detailed analysis of a few millions single stars in the Milky Way and in the Local Group) and cosmology (based on a spectroscopic study of the integrated light from several millions of galaxies at redshifts z>1).
The top-level requirements for the instrument that directly affect the design of the spectrograph are:

- Simultaneous spectroscopy of 800 (goal 1000) objects/sky fibers at one of the VLT foci.
- Sky-projected diameter of each fiber of 1.0 (goal 1.2) arc-sec.
- Medium spectral resolution mode with resolving power R>3,000 (goal R> 4,000) that simultaneously cover the spectral ranges 830-1330 nm (goal 640-1350 nm) and 1470-1750 nm (goal 1450-1800 nm)
- High spectral resolution mode simultaneously covering part of the H band (wavelength range 1523-1620 nm; goal 1521-1632 nm) at resolving power R>18,000 (goal R=23,000) and a region centered on the CaII triplet (wavelength range 765-895 nm; goal 760-900 nm) with resolving power R>9,000 (goal R=10,000).
- Cross-talk between neighboring spectra lower than 2% (goal 1%).

These requirements translate into remarkable challenges for the design of the spectrograph. A detailed analysis of the spectrometer parameters, the preliminary optical design and the trade-off analysis; used for the phase-A proposal and for the PDR; has already been published.[3,4] Here we present the latest version of the design that was developed at the end of the PDR with the specific aim to optimize the optical quality, to simplify the alignment and to minimize the total volume and mass of the spectrometer.

*oliva@arcetri.astro.it; phone +39 0552752291

Ground-based and Airborne Instrumentation for Astronomy VI, edited by Christopher J. Evans, Luc Simard, Hideki Takami
Proc. of SPIE Vol. 9908, 99087R · © 2016 SPIE · CCC code: 0277-786X/16/$18 · doi: 10.1117/12.2231388

2. OVERALL DESIGN OF THE SPECTROGRAPH

The baseline design consists of two identical spectrographs. Each instrument collects the light from 512 fibres. The light from the fibres is collimated and fed, through two dichroics, to three dispersers covering the "RI", "YJ" and "H" arms. The names of these arms correspond to the photometric bands that they cover. The instrument foresees two observing configurations, namely "low resolution" (LR) and "high resolution" (HR). The first provides a complete wavelength-coverage while the second covers selected ranges of specific interest. The wavelength ranges are fixed.

The main optical parameters for the design of the instrument are as follows.

D_{TEL}	Telescope diameter, fixed to 8m (VLT)
d_{PIX}	Pixel size, fixed to 15μm
NX_{PIX}	Total number of pixels along dispersion
NY_{PIX}	Total number of pixels along the slit
N_{FIB}	Total number of fibres aligned along the slit
D_{COLL}	Diameter of the spectrometer collimated beam
F_{CAM}	Focal aperture of the beam on the detector
F_{COLL}	Focal aperture of the collimator and nominal output-focal-ratio of fibres
N_{RES}	Sampling, i.e. diameter of fibre image on detector expressed in pixels
N_{DARK}	Number of dark pixels between adjacent spectra, chosen to be 5/3 of N_{RES}
α_G	Blaze angle of the grating
θ_{FIB}	Sky projected diameter of a fibre
η_{FRD}	Fibre throughput degradation factor = $[(A\Omega)_{TEL}/(A\Omega)_{SPEC}]^{0.5}$

Where $(A\Omega)_{TEL}$ is the etendue at the entrance of the fibre and $/(A\Omega)_{SPEC}$ is the etendue accepted by the spectrometer. Therefore, the parameter η_{FRD} defines by how much the spectrometer is over-sized to compensate for the throughput losses produced by the fibres. Our reference value is η_{FRD} =0.90 and includes the focal ratio degradation and the under-sizing of the fibre illumination necessary to compensate for pupil-wandering at the entrance of the fibre. In other words, the spectrometer is over-sized as if it had to be coupled to a telescope with diameter of 8.8 meters. The derived quantities and scaling laws are as follows.

Sky projected size of pixel	$\theta_{PIX} = 0.36" \ (\eta_{FRD}/0.90) \ (F_{CAM}/0.95)^{-1}$
Diameter of fibre core	$d_{FIB} = 0.15 \ (\theta_{FIB}/1.0") \ (\eta_{FRD}/0.90)^{-1} \ (F_{COLL}/3.5)$ mm
Sampling	$N_{RES} = 2.7 \ (\theta_{FIB}/1.0") \ (F_{CAM}/0.95) \ (\eta_{FRD}/0.90)^{-1}$ pixels
Distance between fibres	$\Delta_{FIB} = 0.40 \ (\theta_{FIB}/1.0") \ (\eta_{FRD}/0.90)^{-1} \ (F_{COLL}/3.5)$ mm
Physical length of input slit	$L_{SLIT} = 205 \ (N_{FIBRES}/512) \ (\theta_{FIB}/1.0") \ (\eta_{FRD}/0.90)^{-1} \ (F_{COLL}/3.5)$ mm
Resolving power ($R=\lambda/\Delta\lambda$)	$R = 13700 \tan(\alpha_G) \ (D_{COLL}/265 \text{ mm}) \ (\theta_{FIB}/1.0")^{-1} \ (\eta_{FRD}/0.90)$
Simultaneous λ–coverage	$\lambda_{MAX} - \lambda_{MIN} = 0.40 \ \lambda_{CENTRAL} \ (NX_{PIX}/4096) \ (R/4000)^{-1} \ (N_{RES}/2.7)^{-1}$

The most striking and demanding aspects for the design of the spectrograph are

- Huge field of view for the collimator, equivalent to a 23' long-slit spectrometer on an 8m telescope.
- Extremely fast cameras with huge field of view, equivalent to a 23' x 23' imager on an 8m telescope.
- High resolution-slit product, achievable only with a large collimated beam that severely limits the use of lenses.
- Simultaneous availability of low and high spectral resolution modes, with simple and affordable exchange modes.

All these challenging requirements are fulfilled in the baseline design of the MOONS spectrometer depicted in Figure 1. The light from the fibers is collimated by a spherical mirror. The input fibers are organized along a curved slit as shown in a previous paper[4]. The collimated beam is split into the three arms by two dichroic beam-splitters. The YJ arm is equipped with a fixed transmission grating that disperses the light. The RI and H arms include interchangeable dispersive systems made by a combination of transmission gratings and prisms; the advantages of this solution are discussed in a previous paper[4].

The dispersed light is re-imaged onto the detector by an extremely compact and remarkably simple camera. It only consists of 2 lenses and one mirror. It achieves truly superb image quality even with focal apertures faster than F/1. For this reason we call it the “Wonder-Camera”.

The main parameters of the spectrometer are summarized in Table 1. They meet all the top level requirements and in several cases reach the goals.

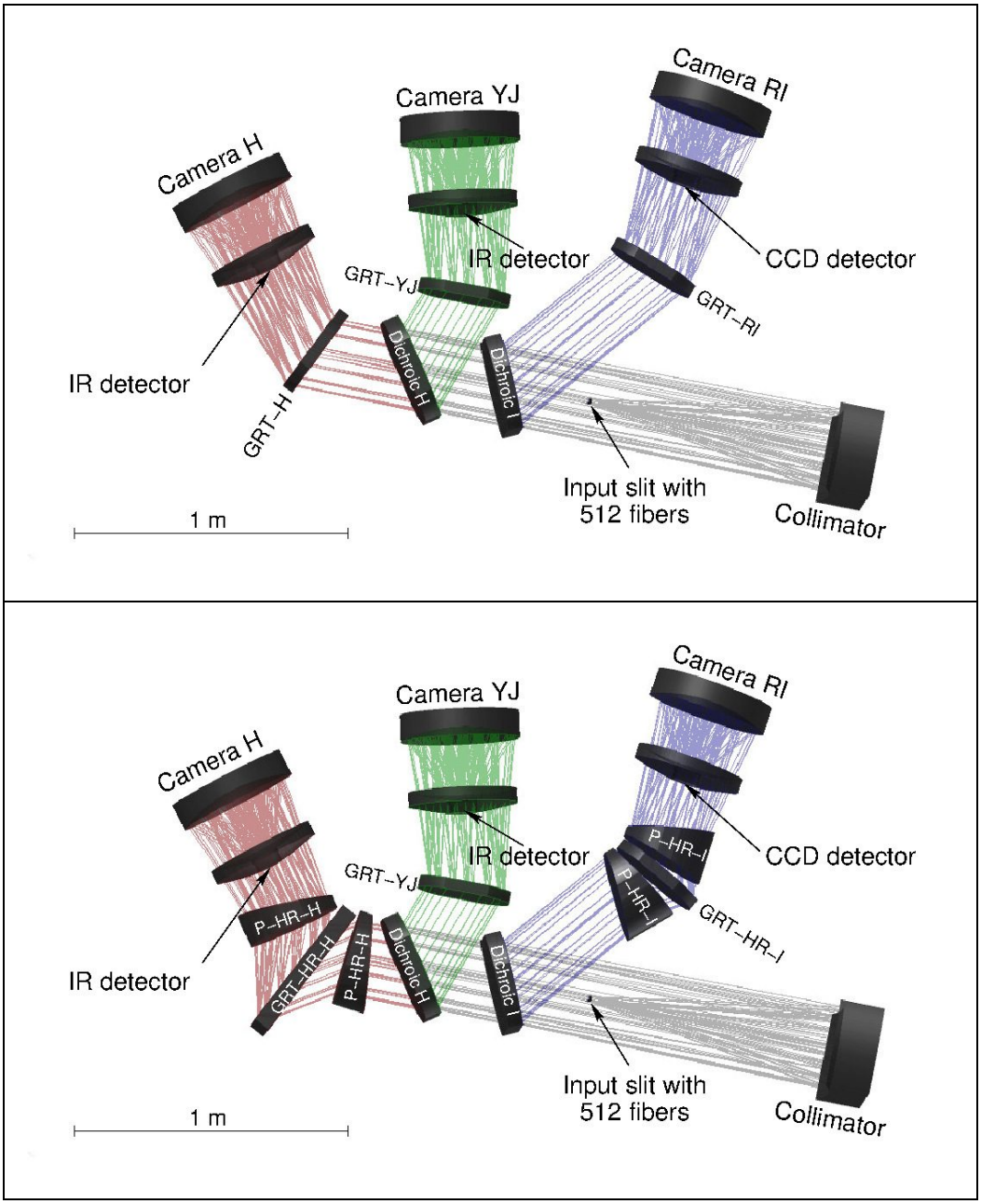

Figure 1 Layout and rays-tracing of the MOONS spectrometer. Top panel: LR configuration, bottom panel: HR configuration.

Table 1 Main parameters of the MOONS spectrometer

Sky projected diameter of a fibre	θ_{FIB} = 1.0"
Focal ratio collimator	F_{COLL} = 3.50
Number of fibres per spectrometer	N_{FIBRES} = 512
Length of input slit	L_{SLIT} = 200 mm
Diameter of collimated beam	D_{COLL} = 265 mm
Focal ratio of the camera	F_{CAM} = 0.95
Sampling	N_{RES} = 2.7 pixels
Number of dark pixels between adjacent fibers	N_{DARK} = 4.5 pixels
Detector size	NX_{PIX} = 4096 NY_{PIX} = 4096 (1 detector per channel)
Simultaneous wavelength coverage and resolving powers in the LR mode	RI arm: 647 – 955 nm R=4500 YJ arm: 934 – 1350 nm R=4300 H arm: 1452 – 1800 nm R=6800
Simultaneous wavelength coverage and resolving powers in the HR mode	RI arm: 765 – 897 nm R=9100 YJ arm: 934 – 1350 nm R=4300 H arm: 1523 – 1640 nm R=18800

3. THE WONDER-CAMERA

Compared to the previous studies[3,4] the most important new feature is the camera. Table 2 summarized the parameters of all cameras included in the trade-off study and Figure 2 shows their layouts. The refractive cameras (RFR) can be conveniently divided into four types.

RFR-H includes only 4 lenses: the first is made of fused-silica and the remaining of mono-crystalline Silicon. It works only in the H band, where Silicon is perfectly transparent. The first surface of L1 is aspheric, the others surfaces are all spherical. Thanks to the very high refractive index of Silicon, this camera can achieve the required optical performances with an overall size and mass similar to the smaller RFL camera. An important drawback is the difficulty to align the lenses, because the Si elements are opaque to optical light and their refractive index strongly varies with temperature.

RFR-IH can be used in all arms and includes 5 lenses: the first and last are made of fused-silica, while the remaining are made of S-FPL51 or CaF_2 (these materials have similar performances in this type of camera). The first surface of L1 and the second surface of L5 are aspheric with quite large departures from a sphere (several mm). Adding aspheres to other surfaces does not help to decrease overall size and volume, but could be useful to achieve milder aspheric profiles on all surfaces. The large size and volume are a direct consequence of the low refractive index of the optical materials. Less bulky cameras can only be obtained by adding lenses with high refractive indices, but unfortunately there is no optical material with high refractive index and transparent over the required wavelength range. Another drawback of this camera is the practical difficulty to limit and control the internal homogeneity of the glass. In the case of fused silica, the homogeneity is normally guaranteed only along the principal axis. Special "3D" manufacturing - that guarantees uniformity along any direction - is possible at an increased cost (factor of 2) but only for relatively small blanks.

RFR-IY is a camera based on "classical glasses". It includes 3 lenses of BK7 and two elements of SF6 (the second and the last lenses). The first surface of L1 and the second surface of L5 are aspheric. This camera can only be used up to about 1150 nm, because of the internal absorption of the glass at longer wavelengths.

CD-RFR-IH is a spectacular example of how the design could be simplified using a curved detector. It consists of only 4 lenses, all of fused silica. The first surface of L1 and the first surface of L3 are elliptical, the remaining surfaces are spherical. The same lenses, with different spacers, can be used for all wavelengths/arms. The fundamental drawback is that curved detectors are not available.

The reflective cameras (RFL) were already discussed in a previous paper[4].

Table 2 Parameters of the cameras considered in the design of the MOONS spectrometer

Name	F/#	Length (mm)	Diameter of largest lens (mm)	Diameter of mirror (mm)	Mass[(1)] (kg)	Central Obs.[(2)] (%)	Comments
Wonder-Camera	0.95	430	400	440	40	19	Detector is inside first lens
RFL-IH-290	1.04	650	440	610	110	17	
RFL-IH-340	1.04	830	520	740	200	13	
RFL-IH-380	1.04	1030	620	920	300	10	
RFR-H	1.05	800	400	-	60	-	
RFR-IH	1.05	930	500	-	230	-	
RFR-IY	1.05	580	420	-	200	-	
CD-RFR-IH	1.00	580	420	-	70	-	Needs a curved detector

Notes to table
(1) Total mass of the optics in one camera.
(2) Fraction of light vignetted by last lens+detector; only for reflective cameras

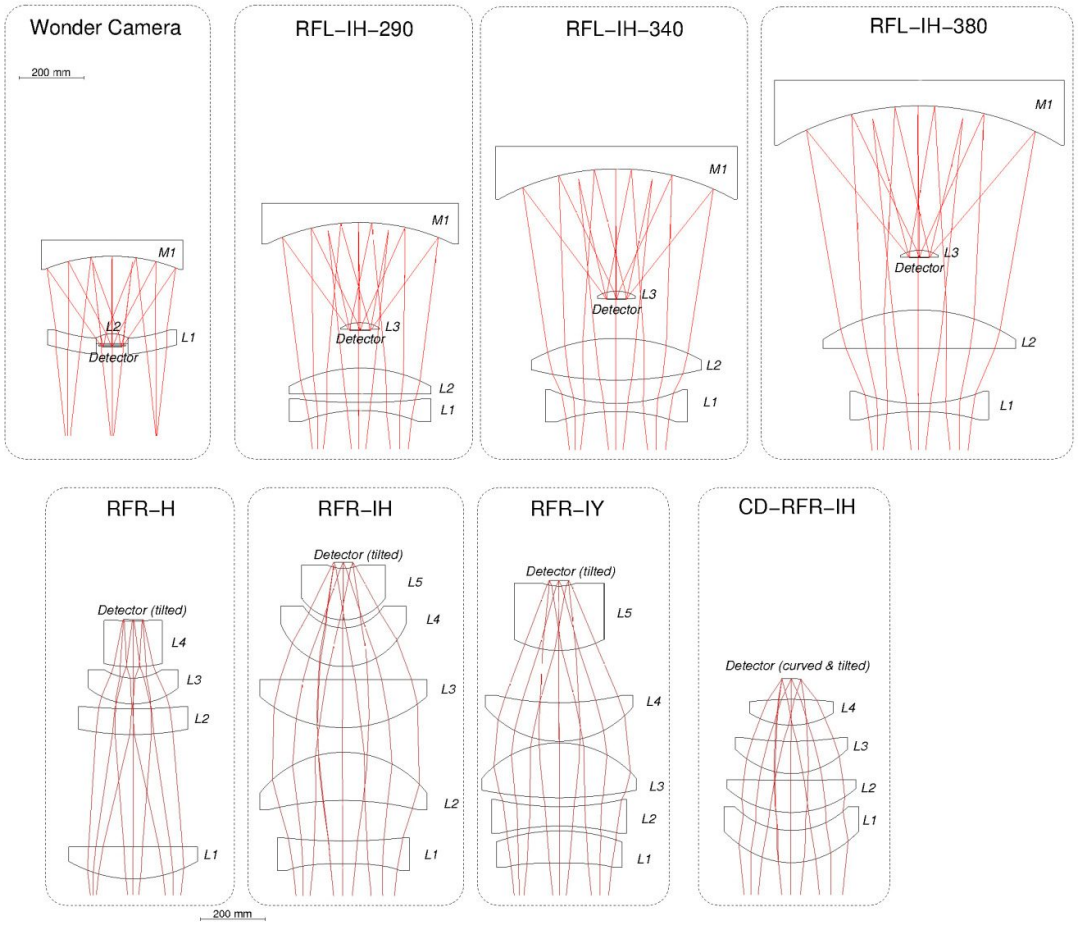

Figure 2 Layout of the Wonder-Camera compared to the other cameras studied for the spectrometer. Light goes from bottom to top.

The Wonder-Camera includes only three aspheric elements, all made of fused silica. The first lens (L1) is a meniscus with a central hole to accommodate the second lens (L2) and the detector (see Figure 3). The last surface of L2 is flat; this simplifies the mounting and interfacing of the two lenses. The clear apertures of the optical elements are within the limits of interferometric scanning metrology systems; thus simplifying manufacturing and quality-control.
The camera achieves its best performance with a quite large back focal distance. Therefore, there is enough room to include long-pass filters made of materials that are intrinsically opaque at shorter wavelengths, i.e. RG glasses for the RI, YJ arms and Silicon for the H arm. This solution is much simpler and cost-effective than using large interference filters in the collimated beam.

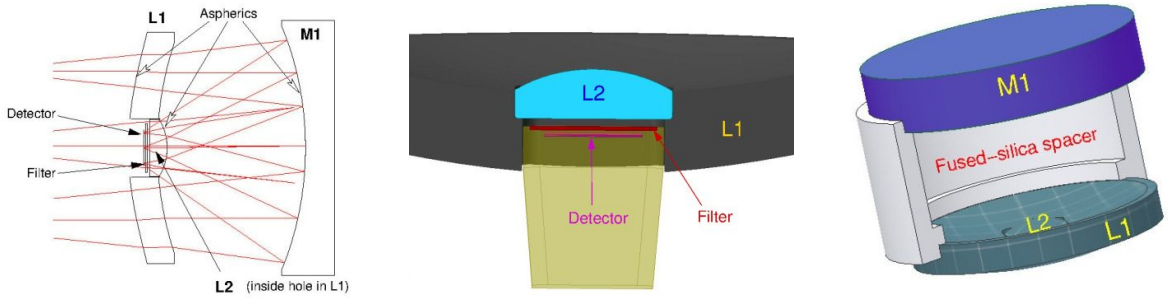

Figure 3 Rays tracing and views of the Wonder-Camera including details of the L1-L2 interface and a possible T-invariant mount.

The optical quality can be evaluated from the plots in Figure 4. Each panel shows the diameters of encircled energy at 50% (green diamonds), 80% (red dots) and 95% (blue crosses) at different wavelengths and spatial positions along the slit for a given observing mode. The Wonder-Camera delivers >95% encircled energy inside the fibre diameter; much better than the image quality achieved with other types of cameras.

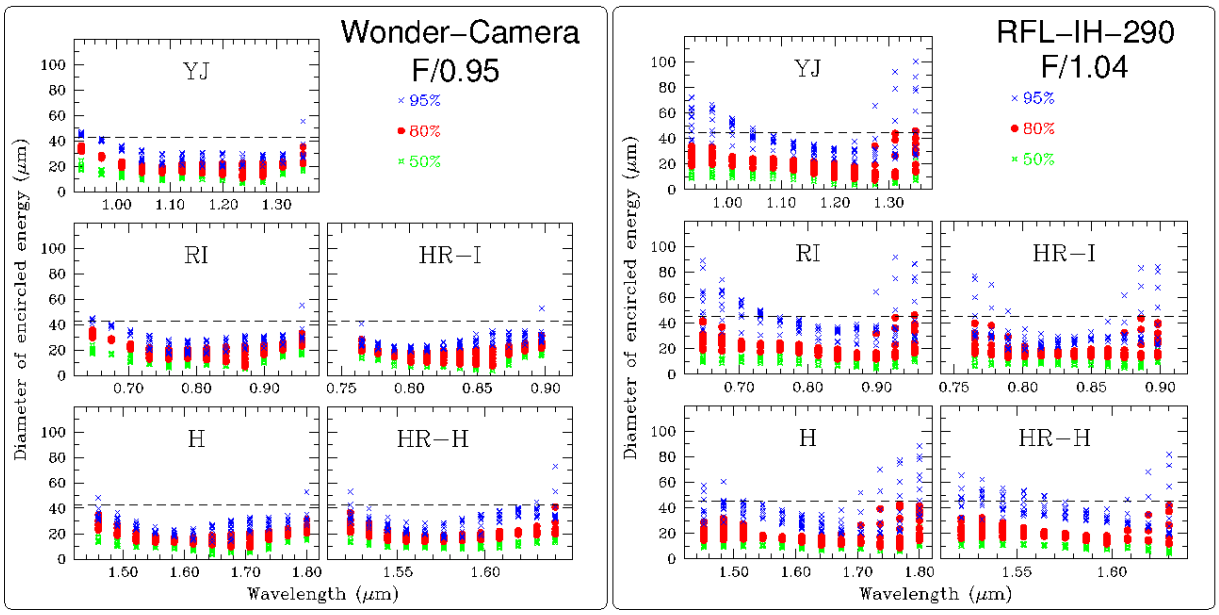

Figure 4 Left panel: optical quality of the Wonder-Camera. Right-hand panel: optical quality of the RFL-IH-290 camera.

The light losses due to the central obscuration are larger than in the other RFL cameras because the latter include a beam-expander that enlarges the beam around the detector[4]. However, the vignetting can be minimized by choosing a very fast focal ratio (F/0.95 in our case). Moreover, the light losses are partly compensated by the smaller number of optical elements (3 instead of 4). The only way to decrease the central obscuration would be using refracting cameras or much larger reflective systems; but these are ruled out because of their excessive sizes, masses and costs.

The Wonder-Camera is relatively simple to align because it consists of only 3 elements of a material (fused silica) with virtually zero thermal expansion coefficients. Moreover change of refractive index with temperature does not affect the optical quality; i.e. the camera has the same performances at room and cryogenic temperatures. Table 3 summarizes the positioning and stability tolerances of the optical elements inside the camera. The tolerances are here defined as the displacements and tilts that produce an increase of 7% of the error-function; a very conservative criterium indeed. The second and third rows are the displacements from the aligned positions that can be recovered by moving (focus + tilt) the detector at operating temperature. The first row, instead, is the accuracy of the initial mounting (gluing) of L2 inside L1: the larger error in Delta-Z (shift along the optical axis) can be corrected by changing the distance between L1 and M1 during the alignment.

It should be noted that the numbers in Table 3 do not refer to the nominal positions of the optics in the optical and CAD designs. Rather, they are the deviations from the "ideal positions" that can be recovered with focus/tilt of the spider-structure holding the filter+detector, without any significant loss of image quality. The "ideal positions" – in particular the distance between L1 and M1 – cannot be defined a-priori, but must be determined during the alignment phase. This is a fundamental characteristic (and complication) of this type of camera. The standard approach of using fixed distances between the optical elements yields manufacturing tolerances (<0.01% on the curvature of M1) that are impossible to meet. Therefore, one must include the possibility of changing (by several mm) the distances between L1 and M1 and align the camera using the following procedure

- Determine the optimal distances between the optical elements; i.e. optimize the optical quality over the whole field of view using a suitable set-up which includes adjustments of all the elements in X,Y,Z,α,β (movements in α,β and X,Y do not need to be independent because lateral shifts and tilts compensate each-other). This procedure can be done at room temperature because the optical quality does not depend on temperature. One must foresee a few mm variations of the distances between L1 and M1.
- Build a holder that maintains the optical elements at the ideal positions (within the tolerances of Table 3) at cryogenic temperatures. This second step could be avoided if the structure used for step-1 is made of fused-silica or other materials with very-low CTEs. In other words, one could most conveniently build a T-invariant mono-block camera mounting/gluing the fused-silica optics onto a fused-silica structure (see Figure 3).
- Correct for residual errors using a cryogenic 3-axis mechanism (focus-tilt) that moves the detector

An alternative possibility, that avoids all the alignment procedure, is adding 3 cryogenic mechanisms/actuators that modify the distance and angle of M1 relative to L1.

Table 3 Positioning and stability tolerances of the elements inside the camera

Elements	Compensators	Delta-Z	Delta-X/Y	Tilt
L2 relative to L1 (for initial mount/gluing)	M1 and detector	0.3 mm	0.1 mm	120 arc-sec
L2 relative to L1 (stability after mounting)	Detector	0.05 mm	0.1 mm	60 arc-sec
M1 relative to L1+L2	Detector	0.05 mm	0.05 mm	30 arc-sec
Filter relative to detector	None	1 mm	5 mm	1 degree
Whole camera relative to disperser	Detector	5 mm	1 mm	360 arc-sec

4. OTHER POSSIBLE APPLICATIONS OF THE WONDER-CAMERA

In this section we briefly describe other possible applications of the Wonder-Camera.

Figure 5 shows the layout of a fast (F/1) wide-field for the E-ELT. It re-images the full field of the E-ELT (D=10 arc-min) onto a D=108 mm focal plane with excellent image quality (80% encircled energy within 15 microns/0.085 arc-sec) over the 450-900 nm spectral range. The central obscuration of the camera is well matched to the central obscuration of the E-ELT, i.e. the camera does not introduce any extra-vignetting.

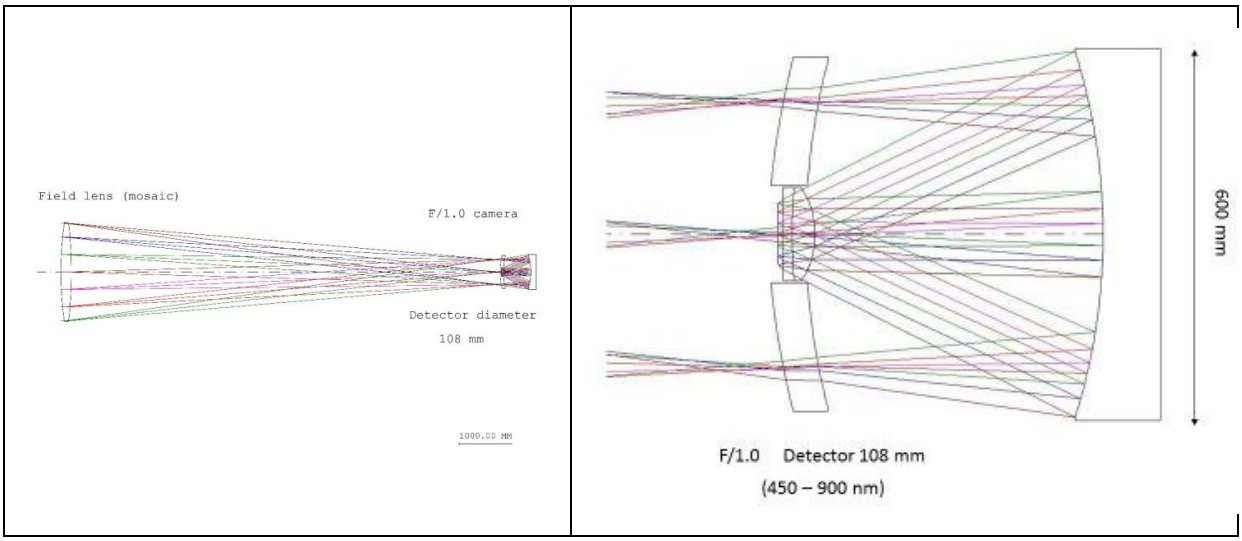

Figure 5 Layout of a F/0.95 wide-field imager for the E-ELT; the design is based on the Wonder-Camera.

A section of the Wonder-Camera could be also used as off-axis optical system without central obscuration. This solution is particularly attractive for applications requiring large optical elements operating at UV and IR wavelengths; because the refractive elements are made of fused-silica, i.e. a material that is intrinsically transparent from below 300 nm to 2500 nm and available in large sizes. Figure 6 shows the layouts of a spectroscopic camera optimized for the UV spectral range and of a complete spectrometer.

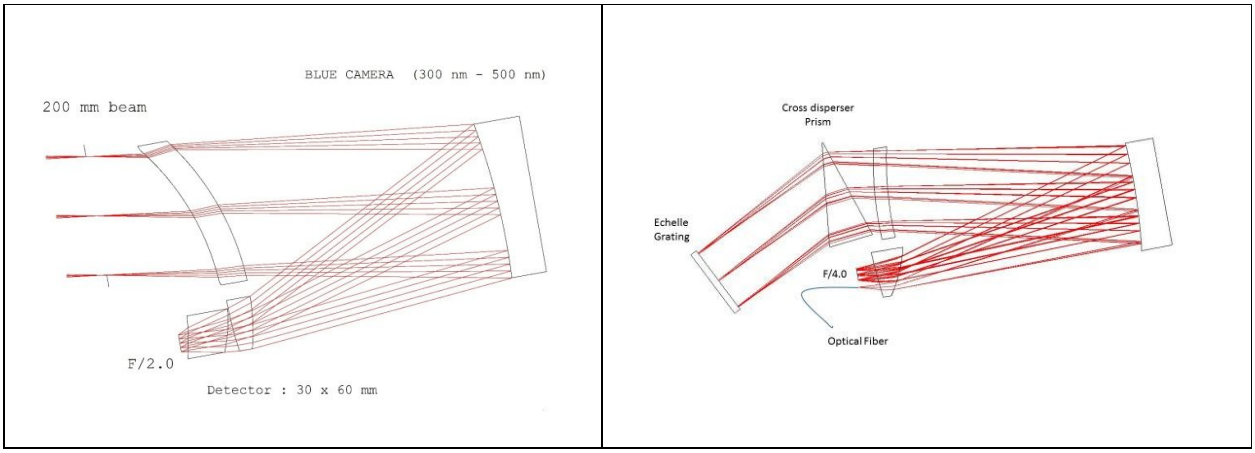

5. ACKNOWLEDGEMENTS

This work was financially supported by the Italian Institute of Astrophysics through the grant and "VLT-PREMIALE"

REFERENCES

[1] Ramsay, S.; Hammersley, P.; Pasquini, L.; The Messenger, 145, 10 (2011)
[2] Cirasuolo, M.; Afonso, J.; Carollo, M.; et al..; SPIE, 9147E-0NC (2014)
[3] Oliva, E.; Diolaiti, E.; Garilli, B.; et al.; SPIE, 8446E-4VO (2012)
[4] Oliva, E.; Todd, S.; Cirasuolo, M.; et al.; SPIE, 9147E-2CO (2014)